Journal of Materials Chemistry C

ROYAL SOCIETY OF CHEMISTRY

PAPER

View Article Online
View Journal

Cite this: DOI: 10.1039/d4tc02806f

Near-infrared emitting single- and mixed-ligand MOFs that can be excited in the visible region: synthesis, crystal structures and sensitization of Nd^{3+}, Er^{3+} and Yb^{3+}†

Athanasia E. Psalti,[a] Despoina Andriotou,[a] Svetlana V. Eliseeva,*[b] Antonios Hatzidimitriou,[a] Stéphane Petoud*[b] and Theodore Lazarides*[a]

Near-infrared (NIR) luminescent lanthanide(III) (Ln^{3+}) metal–organic frameworks (MOFs) constitute a class of materials possessing unique advantages for a wide range of applications due to their photophysical and structural properties. In this work, we present the synthesis and characterization of two series of Ln^{3+}-based MOFs emitting in the NIR region (Ln-MOFs) constructed using 2,6-naphthalene dicarboxylic acid (H_2NDC) and its two amino derivatives, 4-aminonaphthalene-2,6-dicarboxylic acid (H_2ANDC) and 4,8-diaminonaphthalene-2,6-dicarboxylic acid (H_2DANDC). The first series comprises mixed-ligand and mixed-metal MOFs with the general formula $[La_{1-x}Ln_x(NDC)_{1-y}(ANDC)_yCl(DMF)]$ (Ln = Nd^{3+}, Yb^{3+}, x = 0.005–1, y = 0–0.2), while the second series features MOFs corresponding to the formulae $[La_{1-x}Ln_x((NDC)_{1-y}(ANDC)_y)_{1.5}(DMF)_2]\cdot DMF$ (Ln = Nd^{3+}, Er^{3+}, Yb^{3+}, Lu^{3+}, x = 0.1 or 1, y = 0.45 or 1) and $[Ln(DANDC)_{1.5}(DMF)_2]\cdot DMF$ (Ln = Nd^{3+}, Er^{3+}, Yb^{3+}). Detailed studies of the photophysical properties of Ln-MOFs have demonstrated that MOF scaffolds provide an efficient sensitization of NIR-emitting Ln^{3+} ions (η_{sens} up to 38% for Nd^{3+} analogues). In addition, Ln-MOFs possess long Ln^{3+} luminescence lifetimes (up to 12 μs for Yb^{3+} analogues) and exhibit Ln^{3+} luminescence quantum yields comparable with the highest values reported today for NIR-emitting Ln-MOFs. We discuss and compare the photophysical processes that lead to Ln^{3+} sensitization in two series of Ln-MOFs. Most importantly, the studied Ln-MOFs are among the few examples of Ln^{3+}-based NIR-emitting MOFs where Ln^{3+} emission can be sensitized upon excitation in the visible range (up to 450 nm).

Received 2nd July 2024,
Accepted 9th September 2024

DOI: 10.1039/d4tc02806f

rsc.li/materials-c

Introduction

Near-infrared (NIR) luminescent materials have been the subject of intense research over the last few decades primarily in the fields of telecommunications, light emitting diodes, lasers, sensing and biological imaging.[1–4] Thanks to recent major advances in light detection technology, analytical techniques based on luminescence are reaching sensitivity levels comparable to those attained by methods based on radioactive isotopes.[5–8] As a result, optical imaging methods, such as fluorescence microscopy, have gained an increasing importance.[9–11] For instance, today, NIR fluorescence imaging offers molecular specificity, real-time detection, and tissue penetration in the centimeter range.[12–14] Currently, the field of NIR bioimaging agents primarily involves highly conjugated organic fluorophores, which, despite significant success, suffer from important limitations associated with the nature of their fluorescence due to spin-allowed transitions, including small Stokes shifts and short emission lifetimes (typically in the ns range) comparable to those of the biological background (autofluorescence), thus precluding the use of temporal discrimination for the removal of this unwanted signal.[15] Furthermore, organic NIR fluorescent probes very often exhibit strong and rapid photobleaching. They exhibit broad emission bands within the NIR-I imaging window (650–900 nm), while those covering the NIR-II window (1000–1700 nm) are relatively rare.[16,17] In contrast, NIR-emitting trivalent lanthanide ions (Ln^{3+}) such as Nd^{3+}, Er^{3+} and Yb^{3+} display long-lived emission signals (up to several μs), and sharp, atomic-like emission profiles, the wavelengths of which are largely unaffected by the environment around the Ln^{3+} centre.[18] Additionally, Ln^{3+} emission bands lie within the NIR-I and NIR-II imaging windows and thus offer an attractive complementary alternative to organic fluorophores.[19–22] The forbidden nature of most f–f transitions (typical

[a] Department of Chemistry, Aristotle University of Thessaloniki, 54124 Thessaloniki, Greece. E-mail: tlazarides@chem.auth.gr
[b] Centre de Biophysique Moléculaire CNRS UPR 4301, 45071 Orléans Cedex 2, France. E-mail: svetlana.eliseeva@cnrs.fr, stephane.petoud@cnrs-orleans.fr

† Electronic supplementary information (ESI) available. CCDC 2312506–2312511. For ESI and crystallographic data in CIF or other electronic format see DOI: https://doi.org/10.1039/d4tc02806f

absorption coefficients $< 1–10\ M^{-1}\ cm^{-1}$) implies the generation of a low luminescence intensity through direct Ln^{3+} excitation, and thus can only be achieved by the use of high-power sources such as lasers. This limitation can be tackled by the indirect population of f–f excited states *via* energy transfer from highly absorbing organic chromophores which are either in sufficiently close proximity or directly coordinated to Ln^{3+}, an approach known as the ''antenna effect'' or ''Ln^{3+} sensitisation''.[18,23] Despite the existence of a large number of antenna ligands for the efficient sensitisation of visible-emitting Ln^{3+}, the emission quantum yields of NIR-emitting Ln^{3+} complexes are generally modest (typically $\ll$ 1%) because of strong non-radiative deactivation of low-lying f–f excited states by the overtones of high-energy oscillators such as O–H, N–H and C–H bonds that are often present in the vicinity of the Ln^{3+} centre. Approaches to alleviate this limitation include the use of deuterated or fluorinated ligands,[24–27] the synthesis of metallacrowns[28–30] where the Ln^{3+} is encapsulated in a d-metal containing scaffold devoid of high energy oscillators, and the study of dendritic systems.[31–34]

Ln^{3+} metal–organic frameworks (Ln-MOFs) constitute a highly promising class of NIR-emitting materials as they allow incorporation of a large number of antenna ligands and emitting ions per unit volume within a rigid framework. This densification strategy has been proven to be successful for generating sufficiently strong and easily recordable signals despite the limited emission of each individual Ln^{3+} centre.[35–38] An additional attractive feature of Ln-MOFs is the combination of Ln^{3+} luminescence properties and the porosity of their structures, enabling them to potentially host a variety of chemical species. Thus, Ln-MOFs are highly promising platforms for numerous applications such as luminescence sensing,[39–41] ratiometric thermometry,[42–46] anticounterfeiting,[47] encoding applications,[48–54] bioimaging and biosensing.[36,55–59] For the latter applications, it is a major advantage to ensure that the Ln^{3+} emission is sensitised in the visible/NIR region in order to avoid unwanted effects caused by UV irradiation to biological systems and to maximise the penetration of the excitation light within biological tissues and fluids. It is thus important to gain a deeper understanding of the various processes involved in the sensitization of NIR-emitting Ln^{3+} for the rational design of luminescent probes.

In this work, we describe the design, synthesis and photophysical properties of two series (series 1 and 2) of NIR-emitting MOFs incorporating three Ln^{3+} of different natures, Nd^{3+}, Er^{3+} and Yb^{3+} as emitting centres, and the ligands 2,6-naphthalene dicarboxylate (NDC^{2-}), 4-aminonaphthalene-2,6-dicarboxylate ($ANDC^{2-}$) and 4,8-diaminonaphthalene-2,6-dicarboxylate ($DANDC^{2-}$) as Ln^{3+} sensitizers. Series 1 and 2 differ by their structures. In addition to MOFs containing only one type of ligand and metal ion, we have also synthesized mixed-ligand and mixed-metal Ln-MOFs for both series to perform a more detailed systematic investigation of the photophysical processes leading to Ln^{3+} sensitization and of the quenching pathways due to intermetallic Ln–Ln energy transfer. The Ln-MOFs of series 1 can be described by the general formula $[La_{1-x}Ln_x(NDC)_{1-y}(ANDC)_yCl(DMF)]$ (shorthand 1-Ln_xANDC_y, Ln = Nd^{3+}, Yb^{3+}, x = 0.005–1, y = 0–0.2; DMF = dimethylformamide) and those of series 2 can be defined by the general formulae $[La_{1-x}Ln_x((NDC)_{1-y}(ANDC)_y)_{1.5}(DMF)_2]\cdot DMF$ (shorthand 2-Ln_xANDC_y, Ln = Nd^{3+}, Er^{3+}, Yb^{3+}, Lu^{3+}, x = 0.1 or 1, y = 0.45 or 1) and $[Ln(DANDC)_{1.5}(DMF)_2]\cdot DMF$ (shorthand 2-LnDANDC, Ln = Nd^{3+}, Er^{3+}, Yb^{3+}) (Table 1). We demonstrate that the NIR Ln^{3+} emission can be sensitized upon excitation of the ligands at wavelengths up to 450 nm. We discuss how the structural characteristics of these Ln-MOFs impact the energy transfer and Ln^{3+} sensitization processes. Overall, the Ln-MOFs synthesized in this work show promising potential for the design of NIR optical imaging agents for biological applications.

Results and discussion

Synthesis

We synthesized two series of Ln-MOFs (Ln = La^{3+}, Nd^{3+}, Er^{3+}, Yb^{3+}) assembled using the carboxylic acids H_2NDC, H_2ANDC and

Table 1 List of synthesized Ln-MOFs discussed in the main text[a]

Series	Metal (mol%)	Ligand (mol%)	Code	Series	Metal (mol%)	Ligand (mol%)	Code
1	Yb	H_2ANDC		1	Nd	H_2ANDC	
	0.5	20	1-$Yb_{0.005}ANDC_{0.2}$		100	0	1-Nd_1NDC
	1		1-$Yb_{0.01}ANDC_{0.2}$		100	1	1-$Nd_1ANDC_{0.01}$
	2		1-$Yb_{0.02}ANDC_{0.2}$		100	2	1-$Nd_1ANDC_{0.02}$
	5		1-$Yb_{0.05}ANDC_{0.2}$		100	5	1-$Nd_1ANDC_{0.05}$
	10		1-$Yb_{0.1}ANDC_{0.2}$		100	10	1-$Nd_1ANDC_{0.1}$
	15		1-$Yb_{0.15}ANDC_{0.2}$		100	20	1-$Nd_1ANDC_{0.2}$
	20		1-$Yb_{0.2}ANDC_{0.2}$	2	Nd	100	2-Nd_1ANDC_1
	30		1-$Yb_{0.3}ANDC_{0.2}$		Nd	45	2-$Nd_1ANDC_{0.45}$
	50		1-$Yb_{0.5}ANDC_{0.2}$		Er	100	2-Er_1ANDC_1
2	100	100	2-Yb_1ANDC_1		Yb	100	2-Yb_1ANDC_1
	10		2-$Yb_{0.1}ANDC_1$			H_2DANDC	
	Lu	100	2-LuANDC		Er	100	2-ErDANDC
					Nd	100	2-NdDANDC
					Yb	100	2-YbDANDC

[a] General formulae of the Ln-MOFs: $[La_{1-x}Ln_x(NDC)_{1-y}(ANDC)_yCl(DMF)]$ (shorthand 1-Ln_xANDC_y, Ln = Nd^{3+}, Yb^{3+}, x = 0.005–1, y = 0–0.2; DMF = dimethylformamide), $[La_{1-x}Ln_x((NDC)_{1-y}(ANDC)_y)_{1.5}(DMF)_2]\cdot DMF$ (shorthand 2-Ln_xANDC_y, Ln = Nd^{3+}, Er^{3+}, Yb^{3+}, Lu^{3+}, x = 0.1 or 1, y = 0.45 or 1) and $[Ln(DANDC)_{1.5}(DMF)_2]\cdot DMF$ (shorthand 2-LnDANDC, Ln = Nd^{3+}, Er^{3+}, Yb^{3+}).

H_2DANDC (the doubly deprotonated forms of the organic ligands are referred in the main text as NDC, ANDC and DANDC). Ln-MOFs of both series were prepared using modified methods previously described by our group.[60] The synthesis of series 1 Ln-MOFs was performed using Ln^{3+} chlorides as metal sources in combination with the mixtures of H_2NDC/H_2ANDC; the molar ratio of H_2ANDC : H_2NDC was varied from 0 to 0.25 while the total ligand to metal molar ratio was kept at 1 : 1. The reaction was conducted at 110 °C during 24 h in DMF. In addition, we synthesized Yb^{3+}-doped MOFs by adding specified amounts of a standard solution of the dopant in DMF to the reaction mixture. The Ln-MOFs of series 1 can be described by the following formula $[La_{1-x}Ln_x(NDC)_{1-y}(ANDC)_yCl(DMF)]$ (Ln = Nd^{3+}, Yb^{3+}, x = 0.005–1, y = 0–0.2). Series 2 features Nd^{3+}, Er^{3+} and Yb^{3+} Ln-MOFs of the general formulae $([La_{1-x}Ln_x((NDC)_{1-y}(ANDC)_y)_{1.5}(DMF)_2]\cdot DMF$ (x = 0.1 or 1, y = 0.45 or 1) and $[Ln(DANDC)_{1.5}(DMF)_2]\cdot DMF$). They were synthesized by the reaction between the Ln^{3+} nitrates, as the metal sources, with the ligands H_2ANDC and H_2DANDC in a 1 : 1.5 molar ratio in a DMF/H_2O/EtOH 10 : 1 : 1 solvent mixture at 70 °C for 72 h. A detailed list of the synthesized Ln-MOFs is provided in Table 1.

Crystal structures from X-ray diffraction on single crystals

Ln-MOFs of series 1 crystalize in the orthorhombic space group *Pnma*. We have previously reported the crystal structure of the visible light-emitting 1-LaNDC MOF,[60] and here we will only briefly describe the one of 1-NdNDC. The crystal structures of series 1 and 2 Ln-MOFs are summarized in Fig. 1. The Nd^{3+} ion is coordinated to nine atoms, six carboxylate oxygen atoms from the NDC ligand, one oxygen atom from a terminal DMF molecule and two chloride anions. The coordination polyhedron is best described as a tricapped trigonal prism. The metal centres are bridged by the chloride ions and the carboxylate oxygens to form infinite zig–zag chains along the *a* axis. Neighbouring chains are connected by bridging NDC ligands to form a 3D framework with rhombic channels along the *a* axis, which are filled with terminally coordinated DMF molecules.

Single-crystal X-ray analysis of Ln-MOFs from series 2 revealed two closely related structures, associated with the early (*e.g.* Nd^{3+}) and the late (*e.g.* Yb^{3+}) lanthanide(III) ions. The 2-Nd_1ANDC$_1$ MOF crystalizes in the triclinic space group $P\bar{1}$. The Nd^{3+} centre is coordinated with nine oxygen atoms, namely seven from the carboxylate groups of the ANDC ligand and two from the terminally coordinated DMF molecules. The coordination $[NdO_9]$ polyhedron is best described as a distorted capped square antiprism. Two adjacent Nd^{3+} polyhedra form an edge-sharing $[Nd_2O_{16}]$ dimer (Fig. 1d). Neighbouring dimers are bridged by ANDC ligands with hapticities μ_2: η^1–η^2 and μ_2: η^1–η^1 forming a three-dimensional framework with parallelepiped channels along the *a* axis, which are occupied by terminally coordinated and guest DMF molecules.

The Ln-MOFs 2-Yb_1ANDC$_1$ and 2-LuANDC share the general structural characteristics with 2-Nd_1ANDC$_1$, with a few subtle differences attributed to the lanthanide(III) contraction.[61] First, the Yb^{3+} and Lu^{3+} centres are coordinated to a total of eight oxygen atoms, six from carboxylate groups of ANDC and two from the terminally coordinated DMF molecules, with the $[LnO_8]$ coordination polyhedra (Ln = Yb^{3+}, Lu^{3+}) being best described as distorted square antiprisms. Two adjacent polyhedra are bridged by four μ_2: η^1–η^1 carboxylate groups from ANDC ligands to form the dimeric SBU which, in this case, comprises two distinct $[LnO_8]$ coordination polyhedra (Fig. 1e).

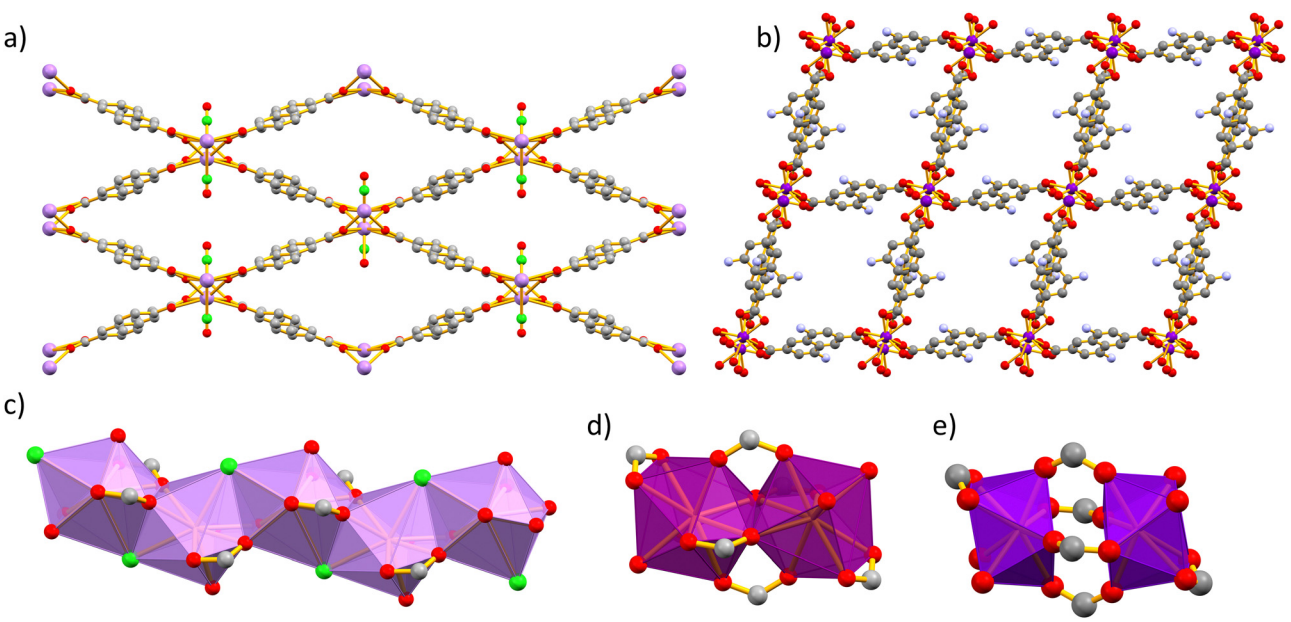

Fig. 1 Crystal structures obtained from X-ray diffraction on single crystals of (a) series 1 Ln-MOFs viewed along the *a* axis and (b) series 2 viewed along the *a* axis (the DMF molecules are omitted for clarity). (c) The zig–zag chain of the $[NdO_8Cl]$ polyhedra of series 1 Ln-MOFs viewed along the *c* axis. (d)–(e) Secondary building units (SBUs) of series 2 Ln-MOFs. Colour code: O: red, C: grey, N: blue, Cl: green, Nd: lilac, Er: magenta, and Yb: purple.

Powder X-ray diffraction

The phase purity of the Ln-MOFs was analyzed by powder X-ray diffraction (PXRD) measurements (Fig. S4 and S5, ESI†). It was demonstrated that 1-Ln_xANDC_y MOFs retained their phase purity up to doping concentrations of $x \leq 0.2$ and $y \leq 0.5$ (Fig. S4, ESI†). Furthermore, when the value of y is more than 0.3, formation of the $P\bar{1}$ phase is preferred. The PXRD patterns of 2-Ln_xANDC_y and 2-LnDANDC are in a good agreement with their respective simulated diagrams. In addition, there is a shift of the diffraction peak appearing at the lowest angle for 2-LnANDC and 2-LnDANDC MOFs that depends on the nature of Ln^{3+} ion. More specifically, the observed peak positions range from 2-theta values equal to 6.85° for Ln = Nd^{3+} to 7.00° for Ln = Er^{3+} and 7.03° for Ln = Yb^{3+}. This observation reflects a slight shrinkage of the MOF, which can be attributed to lanthanide(III) contraction (Fig. S5, ESI†).[61]

Photophysical studies

In order to assess the ability of our new MOFs to sensitize Nd^{3+}, Yb^{3+} and Er^{3+}, steady-state and time-resolved luminescence spectra were collected on microcrystalline samples of Ln-MOFs at room temperature. The absorption spectra of the studied bridging ligands in MeOH solution are given in Fig. 2. H_2NDC displays two structured π–π* absorption bands in the UV range centred at 280 and 340 nm with the absorption tailing off at *ca.* 360 nm. H_2ANDC and H_2DANDC show similar absorption features in the UV range in addition to two substantially red-shifted absorption bands centred at 385 and 412 nm, respectively. The latter features, that tail off at *ca.* 450 (H_2ANDC) and 460 nm (H_2DANDC), can be assigned to charge transfer transitions involving an electron from an orbital localized mainly on the amino group to a vacant π* orbital of the aromatic core.[62]

Representative optical spectra of Ln-MOFs are collected in Fig. 3. Excitation spectra of 2-Nd_1ANDC_1, 2-Er_1ANDC_1 and 2-Yb_1ANDC_1 MOFs upon monitoring of the emission of the respective Ln^{3+} (Nd^{3+}: $^4F_{3/2} \rightarrow {}^4I_{11/2}$ at 1064 nm, Er^{3+}: $^4I_{13/2} \rightarrow {}^4I_{15/2}$ at 1525 nm and Yb^{3+}: $^2F_{5/2} \rightarrow {}^2F_{7/2}$ at 980 nm) exhibit similar broad bands in the range of 250–470 nm (Fig. 3f). This observation confirms that for all three 2-LnANDC MOFs the sensitization of different NIR-emitting Ln^{3+} ions is occurring through the electronic states of the chromophoric ligands. The excitation spectra of 1-Ln_xANDC_y MOFs in the range up to 380 nm are dominated by the bands associated with the 2,6-naphthalene dicarboxylate chromophoric group. The ANDC contribution appears as a shoulder located around 400 nm, which becomes more pronounced as the ANDC content increases (Fig. 3c, d and Fig. S6, ESI†). Additionally, we observed narrow bands that correspond to direct excitation occurring through the f–f transitions of the respective Ln^{3+}. For example, 2-Nd_1ANDC_1 exhibits these narrow excitation bands at 524, 582, 683, 746, 803 and 867 nm that can be attributed to the Nd^{3+} $^4I_{9/2} \rightarrow {}^4G_{7/2}$, $^4G_{5/2}$, $^2H_{11/2}$, $^4F_{9/2}$, $^4F_{7/2} + {}^4S_{3/2}$ and $^4F_{5/2} + {}^2H_{9/2}$ transitions, respectively. 2-ErANDC shows the Er^{3+}-based narrow excitation bands at 520 and 656 nm arising from the $^4I_{15/2} \rightarrow {}^2H_{11/2}$, $^4F_{9/2}$ transitions, respectively. On the other hand, no such sharp features are observed in the excitation spectrum of 2-YbANDC since Yb^{3+} does not possess any electronic levels in the UV-visible range.

Upon excitation of the chromophoric ligands at 400 nm, 2-LnANDC MOFs (Ln = Nd, Er, Yb) exhibit characteristic Ln^{3+} luminescence signals indicating that the ligand sensitizes all three NIR-emitting Ln^{3+} ions *via* the antenna effect (Fig. 3g). In particular, the emission spectrum of 2-NdANDC revealed the presence of the Nd^{3+} bands centred at 873, 1056 and 1330 nm, attributed to the $^4F_{3/2} \rightarrow {}^4I_{9/2}$, $^4I_{11/2}$, and $^4F_{3/2} \rightarrow {}^4I_{13/2}$ electronic transitions, while those of 2-ErANDC and 2-YbANDC exhibit the Er^{3+} (centered at 1514 nm) and Yb^{3+} (centered at 978 nm) emission bands attributed to the $^4I_{13/2} \rightarrow {}^4I_{15/2}$ and $^2F_{5/2} \rightarrow {}^2F_{7/2}$ transitions, respectively. The 2-LnDANDC MOFs show similar behaviour (Fig. 3h–i) with respect to the sensitization of NIR-emitting Ln^{3+}. In addition, both series of Ln-MOFs containing DANDC or ANDC ligands exhibit residual broad-band ligand-centred emission in the visible range centred at 480 and 500 nm, respectively (Fig. 3e), indicating that the energy transfer from the MOF sensitizers to the Ln^{3+} is incomplete for all three Ln^{3+} cations investigated in this work.

We further investigated the contribution of the NDC ligand on the sensitization of NIR-emitting Ln^{3+} by analyzing the photophysical properties of the mixed-ligand Ln-MOFs, *i.e.* 1-Nd_1ANDC_y (y = 0–0.2) and 1-$Yb_xANDC_{0.2}$ (x = 0.005–0.5). We observed that, in both cases, upon excitation either into the NDC-centred bands at 350 nm or into the ANDC-centred bands at 415 nm, the characteristic emissions of Nd^{3+} and Yb^{3+} in the NIR range are generated (Fig. 3a and b and Fig. S6, S7, ESI†). This observation indicates that NDC contributes to the sensitization of the NIR-emitting Ln^{3+} either directly or indirectly *via* an NDC-to-ANDC energy transfer.[60] Excitation spectra of 1-Ln_xANDC_y MOFs (Fig. 3c and d) exhibit similar ligand-centred spectral features as the ones observed in the diffuse reflectance spectra further confirming Ln^{3+} sensitization through the Ln-MOF ligands. Moreover, in the case of 1-Nd_xANDC_y MOFs,

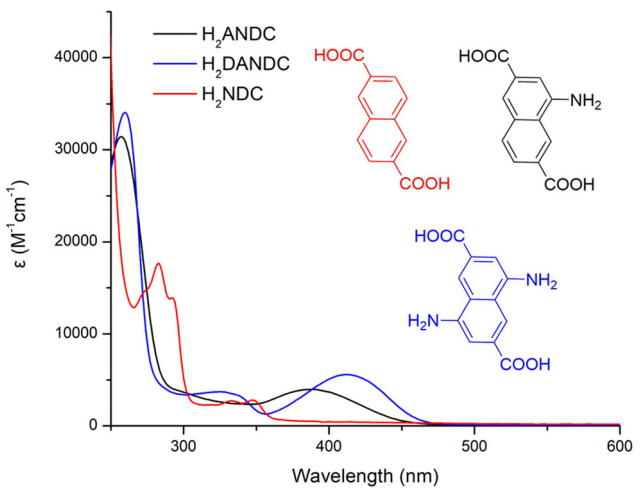

Fig. 2 Absorption spectra of the ligands H_2NDC, H_2ANDC and H_2DANDC in MeOH (10^{-5} M).

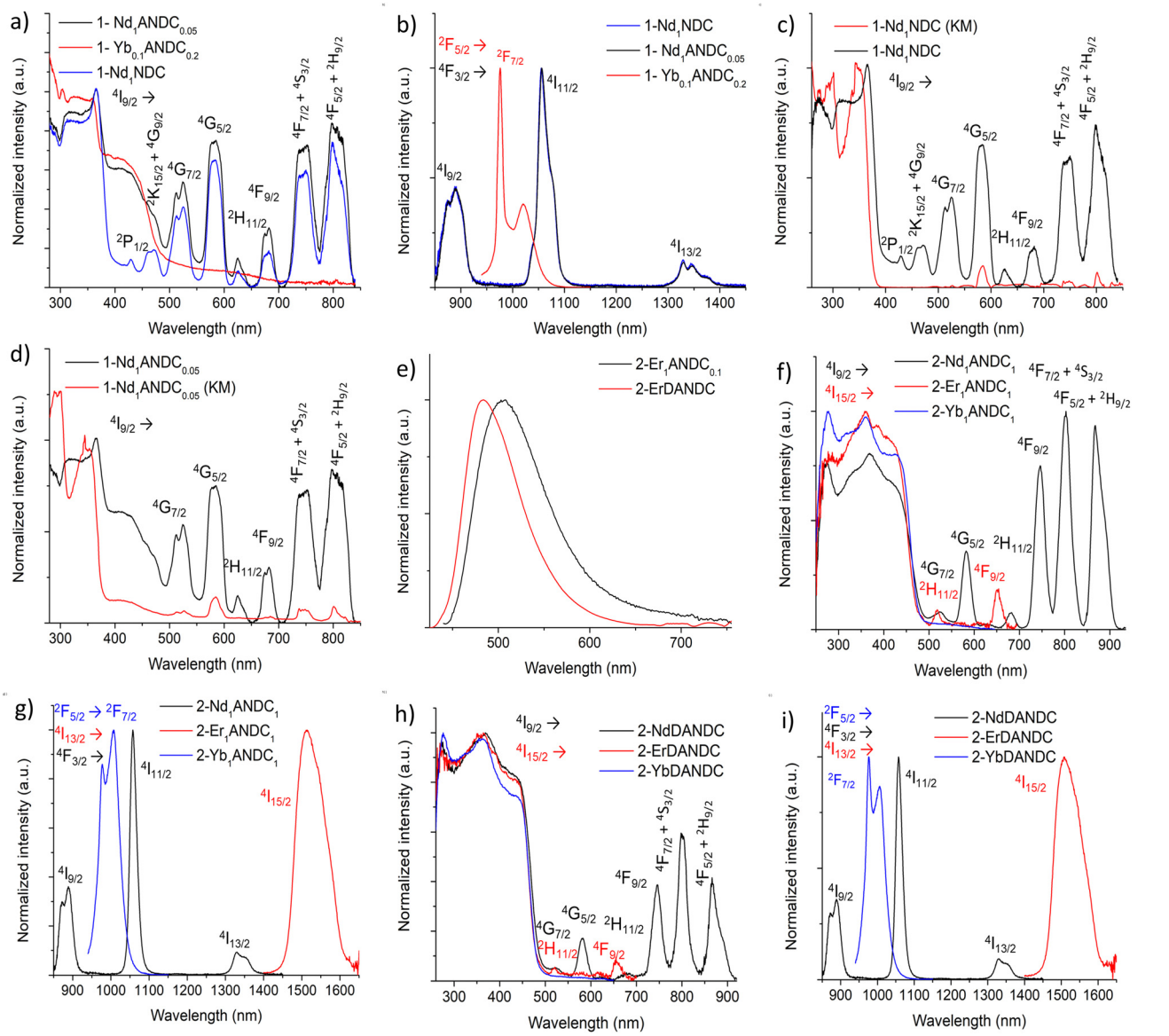

Fig. 3 (a) Excitation spectra of 1-$Nd_1ANDC_{0.05}$, 1-$Yb_{0.1}ANDC_{0.2}$ and 1-Nd_1NDC. (b) Emission spectra of 1-Nd_1NDC, 1-$Nd_1ANDC_{0.05}$ and 1-$Yb_{0.1}ANDC_{0.2}$ (λ_{exc} = 350 nm). Overlay of excitation and diffuse reflectance spectra, after conversion to Kubelka–Munk (KM) function, for (c) 1-Nd_1NDC and (d) 1-$Nd_1ANDC_{0.05}$. (e) Representative ligand-centred emission spectra of 2-$Er_1ANDC_{0.1}$ and 2-ErDANDC (λ_{exc} = 400 nm). (f) Excitation spectra of 2-Nd_1ANDC_1, 2-Er_1ANDC_1 and 2-Yb_1ANDC_1 and (g) emission spectra of 2-Nd_1ANDC_1, 2-Er_1ANDC_1 and 2-Yb_1ANDC_1 (λ_{exc} = 400 nm). (h) Excitation spectra of 2-NdDANDC, 2-ErDANDC and 2-YbDANDC and (i) emission spectra of 2-NdDANDC, 2-ErDANDC and 2-YbDANDC (λ_{exc} = 400 nm). The excitation spectra were recorded upon monitoring the emission maximum of the corresponding Ln^{3+}. All spectra were corrected for detector response and normalized.

sharp features corresponding to the Nd^{3+} transitions are observed. It should be noted that the band located in the range 400–450 nm, attributed to the presence of the ANDC ligand, becomes more pronounced upon increasing the ANDC content in the 1-Ln_xANDC_y MOFs (Fig. S6 and S7, ESI†). The absolute quantum yields of Ln^{3+} emission under excitation into the electronic levels of the chromophoric ANDC and DANDC ligands (Φ^{L}_{Ln}) were collected for all relevant Ln-MOFs (Table 2). It was found that for 1-$NdANDC_y$ (y = 0.05–0.2) MOFs the ANDC loading level has no effect on the Nd^{3+} emission quantum yields even when the excitation takes place selectively on the ANDC chromophore. This observation potentially reflects the presence of a mechanism in which initial ANDC excitation is followed by the thermal equilibration of the NDC and ANDC triplet (T_1) levels ($\Delta E \approx 1600\ cm^{-1}$, *vide infra*), with both acting as sensitizers for Nd^{3+}. In contrast to 1-$NdANDC_y$ MOFs, the quantum yields of the Yb^{3+}-based emission in mixed-metal Yb/La-MOFs with x = 0.1 show significant dependence on the ANDC loading. Notably, there is a ten-fold increase of the Yb^{3+} emission quantum yield, upon excitation at 410 nm, between 1-$Yb_{0.1}ANDC_{0.2}$ and 2-$Yb_{0.1}ANDC_1$ where the ANDC content increases from 20 to 100 mol%. This can be

Table 2 Ln^{3+}-centred luminescence quantum yields (Φ^{L}_{Ln}) and observed luminescence lifetimes (τ_{obs}) of the studied Ln-MOFs in the solid state[a]

Ln-MOF	$\Phi^{L}_{Ln}(10^{-2}\%)$[b]	τ_{obs} (μs)[c]
1-NdNDC	13.03(6)[c]	1.035(4)
1-Nd_1ANDC$_{0.01}$	12.2(4)[c]	1.032(3)
1-Nd_1ANDC$_{0.02}$	10.5(1)[c]	1.06(1)
1-Nd_1ANDC$_{0.05}$	9.52(7)	1.08(1)
1-Nd_1ANDC$_{0.1}$	10(7)	1.072(8)
1-Nd_1ANDC$_{0.2}$	10.8(1)	1.03(1)
2-Nd_1ANDC	11.5(2)	0.96(1)
2-Nd_1ANDC$_{0.45}$	17.3(2)	0.957(6)
2-Nd_1ANDC$_{0.1}$	8.1(2)	1.018(5)
2-Nd_1DANDC	7.2(5)	0.81(4)
1-$Yb_{0.005}$ANDC$_{0.2}$	0.10(1)	N/A
1-$Yb_{0.01}$ANDC$_{0.2}$	0.116(9)	1.349(8)
1-$Yb_{0.02}$ANDC$_{0.2}$	0.24(1)	14.9(1)
1-$Yb_{0.05}$ANDC$_{0.2}$	0.58(2)	14.3(1)
1-$Yb_{0.1}$ANDC$_{0.2}$	1.56(2)	14.8(4)
1-$Yb_{0.15}$ANDC$_{0.2}$	2.46(5)	15.63(6)
1-$Yb_{0.2}$ANDC$_{0.2}$	5.41(5)	15.09(8)
1-$Yb_{0.3}$ANDC$_{0.2}$	0.880(1)	14.4(1)
1-$Yb_{0.5}$ANDC$_{0.2}$	1.93(2)	12.1(4)
2-$Yb_{0.1}$ANDC$_1$	13.6(3)	11.35(2)
2-Yb_1ANDC$_1$	14.7(3)	9.68(2)
2-YbDANDC	21.4(5)	8.11(4)
2-ErANDC	0.73(4)	1.68(2)
2-ErDANDC	0.48(5)	1.27(1)

[a] Data obtained at room temperature. Standard deviation (2σ) is between parentheses; estimated relative errors: τ_{obs}, ±2%; Φ^{L}_{Ln}, ±10%. [b] Under excitation at 400–410 nm. [c] Under excitation at 355 nm.

mainly attributed to the more efficient ANDC-Yb^{3+} interaction in 2-$Yb_{0.1}$ANDC$_1$ since effectively all Yb^{3+} ions are directly connected to an ANDC sensitizer. On the other hand, the Yb^{3+} emission quantum yields and lifetimes are comparable for 2-Yb_1ANDC$_1$ and 2-$Yb_{0.1}$ANDC$_1$ MOFs (Table 2) indicating that there is no significant Yb–Yb quenching pathway.

In addition, for 2-Nd_1ANDC$_1$, 2-Nd_1ANDC$_{0.1}$ and 2-NdDANDC MOFs, the intrinsic quantum yields of the Nd^{3+} emission under direct excitation into its f–f transition at 750 nm (Φ^{Ln}_{Ln}) could be acquired and were found to be 0.307(7) %, 0.293(1) % and 0.201(1) %, respectively. Using the values of Φ^{Ln}_{Ln} and Φ^{L}_{Ln}, we calculated the sensitization efficiencies of Nd^{3+} (η_{sens}) according to the formula:

$$\Phi^{Ln}_{Ln} = \eta_{sens} \times \Phi^{Ln}_{Ln}$$

We found that the values of η_{sens} are similar for 2-Nd_1ANDC$_1$ and 2-NdDANDC (38 ± 8% *vs.* 35 ± 5%) and slightly lower for 2-NdANDC$_{0.1}$ (27 ± 1%).

Experimental luminescence decay curves of Ln-MOFs (Ln = Yb^{3+}, Nd^{3+}, Er^{3+}) measured under excitation of the chromophoric sensitizers (λ_{ex} = 355 nm) and upon monitoring the NIR emission signals arising from the main transitions of the corresponding Ln^{3+} (Nd^{3+}: $^4F_{3/2} \rightarrow {}^4I_{11/2}$ at 1064 nm, Er^{3+}: $^4I_{13/2} \rightarrow {}^4I_{15/2}$ at 1525 nm and Yb^{3+}: $^2F_{5/2} \rightarrow {}^2F_{7/2}$ at 980 nm) are best fitted with a monoexponential function. Such behaviour indicates that Ln^{3+} ions are located in a single well-defined coordination environment within the MOF scaffold. The measured values of the observed luminescence lifetimes (τ_{obs}) are in the order of 1 μs for Nd^{3+} MOFs and range between 10 and 15 μs for the MOFs incorporating Yb^{3+} (Table 2). The similarity of the values of τ_{obs} for a particular Ln^{3+} within the studied series of MOFs suggests that they are insignificantly affected by the nature of the ligands and their content in Ln-MOFs. The values of τ_{obs} are comparable with the ones reported for similar NIR-emitting Ln-MOFs.[63,64]

Ligand-centred photophysical properties and the Ln^{3+} sensitization mechanism

To further investigate the energy transfer processes that take place between NDC, its amino- derivatives, and the Ln^{3+} ions within the Ln-MOF matrices, we conducted steady-state and time-gated luminescence analysis at a low temperature (77 K) of the 1-Nd_1NDC, 1-LaANDC$_{0.02}$ and 1-LaDANDC$_{0.02}$ MOFs. The energy of an excited state is defined as the energy gap between the lowest vibrational level of the excited state and that of the corresponding ground state (the so-called 0–0 energy gap). Spectroscopically, this energy is quantified by identifying the 0–0 transition at low temperature as the highest-energy vibrational feature of the corresponding emission signal. Consequently, the energy of the lowest spin-allowed (S_1) excited state is determined by deconvoluting the fluorescence spectrum measured at 77 K. Similarly, the energy of the long-lived lowest spin-forbidden state (T_1) can be quantified from the corresponding phosphorescence spectrum which is measured in a time-gating mode by applying a delay of *ca.* 1 μs to remove short-lived fluorescence signals. Using the described method, we determined the energies of the ligands' excited states by performing Gaussian deconvolution of the emission spectra of the mixed-ligand Ln-MOFs acquired at 77 K in the steady-state mode for the S_1 excited states and in the time-gated mode for the T_1 excited states (Fig. S11, ESI†).[65] The energy diagram of Fig. 4 shows that the excited levels, including the long-lived T_1 states of NDC, ANDC and DANDC, lie above the main emissive levels of Nd^{3+} ($^4F_{3/2}$), Er^{3+} ($^4I_{13/2}$) and Yb^{3+} ($^2F_{5/2}$), therefore, are in favourable energy positions to populate them.[66]

In general, the sensitization of the Ln^{3+} in the studied series of MOFs involves the excitation of the electronic states of the NDC chromophore, since it is a dominant one in the matrix, thus creating a ligand excited state (exciton). Then, this excited state migrates through the matrix by a series of energy transfer steps (exciton hoping) until it reaches an energy acceptor site (either an amino-substituted ligand, *i.e.* ANDC or DANDC, or a low-lying excited state of Ln^{3+}), or it eventually decays through radiative or non-radiative (thermal) processes.[67] To gain insight into the process of energy transfer from NDC to its amino derivatives, ANDC and DANDC, we measured and analysed the NDC-centred quantum yields (Φ^{L}) of 1-LaANDC$_y$ and 1-LaDANDC$_y$ with low doping levels of amino-substituted derivatives (y = 0–0.002) under excitation at 330 nm (experimental details in the ESI† and results in Table S3). This process allowed the achievement of partial NDC-to-(D)ANDC energy transfer, which is readily quantifiable with our experimental setup, instead of the almost complete quenching of NDC-centred emission which is observed in Ln-MOFs with higher acceptor loadings. We plotted the ratios of the quantum yield

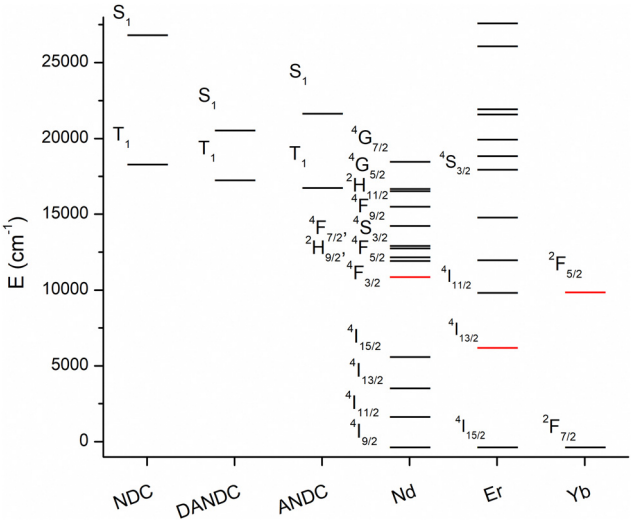

Fig. 4 Energy diagram of the singlet (S_1) and triplet (T_1) excited states of the NDC, ANDC and DANC ligands and the electronic levels of the Ln^{3+} ions (red: emissive levels).

values obtained for the 1-LaNDC MOF (Φ_0^L) over the ones acquired for 1-LaANDC$_y$ and 1-LaDANDC$_y$ (Φ^L) MOFs against the molar fraction of ANDC and DANDC within the MOF in order to construct a Stern–Volmer type plot (Fig. 5).[67] In both cases, the quantum yield of the NDC-centred emission decreases progressively upon addition of a quencher (ANDC or DANDC) due to the incorporation of more low-energy acceptor sites into the MOF. We found that the slopes observed in the Stern–Volmer plots for 1-LaANDC$_y$ and 1-LaDANDC$_y$ are in the same order of magnitude. The steeper slope for the latter possibly indicates that the energy transfer efficiency from the NDC ligand is more efficient for the DANDC ligands than for the ANDC ones.[68,69]

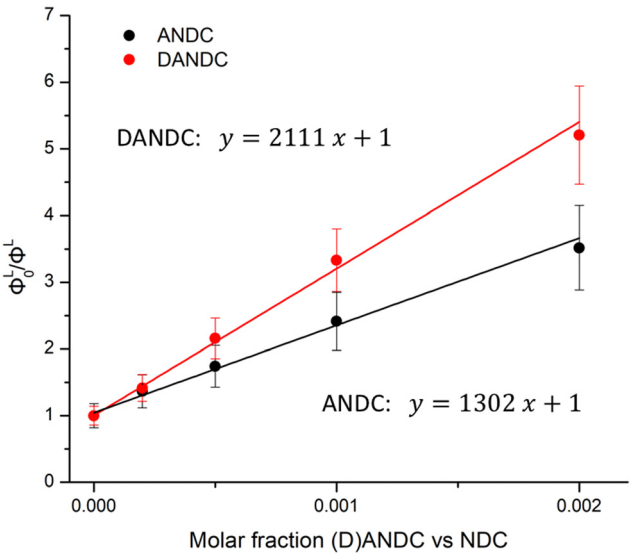

Fig. 5 Stern–Volmer-type plots of Φ_0^L/Φ^L for LaANDC$_y$ and LaDANDC$_y$ over the molar fractions of ANDC (red) and DANDC (black) (y = 0–0.002) in the MOF ($R^2 > 0.996$). The values of the corresponding quantum yields are given in Table S3 (ESI†).

Conclusions

In summary, we have synthesized two new series of Ln-MOFs (Ln = La^{3+}, Nd^{3+}, Er^{3+}, Yb^{3+}, Lu^{3+}) featuring H_2NDC and its amino derivatives, H_2ANDC and H_2DANDC, with the general formulae $[La_{1-x}Ln_x(NDC)_{1-y}(ANDC)_yCl(DMF)]$ (Ln = Nd^{3+}, Yb^{3+}, x = 0.005–1, y = 0–0.2) (series 1) and $[La_{1-x}Ln_x((NDC)_{1-y}(ANDC)_y)_{1.5}(DMF)_2]\cdot DMF$ (Ln = Nd^{3+}, Er^{3+}, Yb^{3+}, Lu^{3+}, x = 0.1 or 1, y = 0.45 or 1), $[Ln(DANDC)_{1.5}(DMF)_2]\cdot DMF$ (Ln = Nd^{3+}, Er^{3+}, Yb^{3+}) (series 2). Series 1 comprises Ln-MOFs with an orthorhombic structure, while the Ln-MOFs of series 2 adopt a triclinic structure. We have demonstrated that series 1 retains its structural integrity upon incorporation of amino-substituted ligands for $y \leq 0.3$, while for higher loadings formation of the triclinic phase is preferred. In addition, Ln-MOFs constructed using 100 mol% H_2ANDC and H_2DANDC ligands crystallize in the triclinic phase with small structural variations pertinent to the lanthanide(III) contraction.[61] In particular, Nd^{3+} and Er^{3+} in the aforementioned Ln-MOFs are nine-coordinated while Yb^{3+} and Lu^{3+} are eight-coordinated. Thus, the secondary building units of the former Ln^{3+} consist of edge sharing $[Ln_2O_{16}]$ dimers while Yb^{3+} and Lu^{3+} form two discrete carboxy-bridged coordination polyhedra. The photophysical analysis of the Ln-MOFs of series 1 revealed that each of the three chromophoric ligands studied in this work is efficient for the sensitization of three different lanthanide(III) cations emitting in the NIR domain, Nd^{3+}, Yb^{3+} and Er^{3+}. This is a major result as the chromophoric ligands that combine absorption in the visible region with the ability to sensitize NIR-emitting Ln^{3+} within a MOF scaffold remain scarce. In mixed-ligand Ln-MOFs, both NDC and ANDC contribute to the sensitization of NIR-emitting Ln^{3+}. An increase of the ANDC content in these Ln-MOFs has a beneficial effect on the Nd^{3+} and Yb^{3+} emission quantum yields. The Nd^{3+} sensitization efficiencies of the series 2 Ln-MOFs were found to be similar for 2-Nd$_1$ANDC$_1$ and 2-NdDANDC, ranging within 35–38%. Overall, this work demonstrates that the use of amino-derivatives of 2,6-naphthalene dicarboxylic acid (H_2NDC) in the construction of Ln-MOFs results in shifting the absorption wavelength to the visible region while achieving efficient sensitization of NIR-emitting Ln^{3+} ions.

Experimental

All experimental information (synthesis, characterization data, X-ray crystallography, instrumentation and software used) are provided in the ESI.†

Conflicts of interest

There are no conflicts to declare.

Acknowledgements

The research work in Greece was supported by the Hellenic Foundation for Research and Innovation (HFRI) under the 3rd Call for HFRI PhD Fellowships (Fellowship Number: 6322). The work in France was partially supported by the 'Ligue Regionale

Contre le Cancer' (comités du Loiret, d'Eure-et-Loir, du Loir-et-Cher and de la Sarthe), the network 'Molecules marines, metabolisme et cancer' from the Canceropôle Grand Ouest. S. P. acknowledges support from the Institut National de la Santé et de la Recherche Medicale (Inserm).

Notes and references

1 J.-C. G. Bünzli and C. Piguet, *Chem. Soc. Rev.*, 2005, **34**, 1048–1077.
2 S. V. Eliseeva and J.-C. G. Bünzli, *Chem. Soc. Rev.*, 2010, **39**, 189–227.
3 A. Mech, A. Monguzzi, F. Meinardi, J. Mezyk, G. MacChi and R. Tubino, *J. Am. Chem. Soc.*, 2010, **132**, 4574–4576.
4 M. D. Ward, *J. Solid State Electrochem.*, 2005, **9**, 778–787.
5 G. T. Dempsey, J. C. Vaughan, K. H. Chen, M. Bates and X. Zhuang, *Nat. Methods*, 2011, **8**, 1027–1036.
6 V. Ntziachristos, C. Bremer and R. Weissleder, *Eur. Radiol.*, 2003, **13**, 195–208.
7 G. T. Dempsey, J. C. Vaughan, K. H. Chen, M. Bates and X. Zhuang, *Nat. Methods*, 2011, **8**, 1027–1036.
8 R. Rigler, M. Orrit and T. Basché, *Single molecule spectroscopy: Nobel conference lectures*, Springer Science & Business Media, 2012, vol. 67.
9 Z. Yang, A. Sharma, J. Qi, X. Peng, D. Y. Lee, R. Hu, D. Lin, J. Qu and J. S. Kim, *Chem. Soc. Rev.*, 2016, **45**, 4651–4667.
10 B. Hötzer, I. L. Medintz and N. Hildebrandt, *Small*, 2012, **8**, 2297–2326.
11 G. D. Luker and K. E. Luker, *J. Nucl. Med.*, 2008, **49**, 1–4.
12 C. Ding and T. Ren, *Coord. Chem. Rev.*, 2023, **482**, 215080.
13 R. Weissleder and V. Ntziachristos, *Nat. Med.*, 2003, **9**, 123–128.
14 X. Dang, N. M. Bardhan, J. Qi, L. Gu, N. A. Eze, C.-W. Lin, S. Kataria, P. T. Hammond and A. M. Belcher, *Sci. Rep.*, 2019, **9**, 3873.
15 J. R. Lakowicz, *Principles of Fluorescence Spectroscopy*, Springer, US, 2007.
16 J. Mu, M. Xiao, Y. Shi, X. Geng, H. Li, Y. Yin and X. Chen, *Angew. Chem., Int. Ed.*, 2022, **61**, e202114722.
17 A. L. Antaris, H. Chen, K. Cheng, Y. Sun, G. Hong, C. Qu, S. Diao, Z. Deng, X. Hu, B. Zhang, X. Zhang, O. K. Yaghi, Z. R. Alamparambil, X. Hong, Z. Cheng and H. Dai, *Nat. Mater.*, 2016, **15**, 235–242.
18 J.-C. G. Bünzli, *Coord. Chem. Rev.*, 2015, **293–294**, 19–47.
19 E. Baggaley, J. A. Weinstein and J. A. G. Williams, *Coord. Chem. Rev.*, 2012, **256**, 1762–1785.
20 A. D'Aléo, A. Bourdolle, S. Brustlein, T. Fauquier, A. Grichine, A. Duperray, P. L. Baldeck, C. Andraud, S. Brasselet and O. Maury, *Angew. Chem., Int. Ed.*, 2012, **51**, 6622–6625.
21 G.-Q. Jin, Y. Ning, J.-X. Geng, Z.-F. Jiang, Y. Wang and J.-L. Zhang, *Inorg. Chem. Front.*, 2020, **7**, 289–299.
22 C. Li, Y. Pang, Y. Xu, M. Lu, L. Tu, Q. Li, A. Sharma, Z. Guo, X. Li and Y. Sun, *Chem. Soc. Rev.*, 2023, **52**, 4392–4442.
23 M. D. Ward, *Coord. Chem. Rev.*, 2010, **254**, 2634–2642.
24 A. S. Hyre and L. H. Doerrer, *Coord. Chem. Rev.*, 2020, **404**, 213098.
25 T. M. George, S. Varughese and M. L. P. Reddy, *RSC Adv.*, 2016, **6**, 69509–69520.
26 G. A. Hebbink, D. N. Reinhoudt and F. C. J. M. van Veggel, *Eur. J. Org. Chem.*, 2001, 4101–4106.
27 G.-Q. Jin, D. Sun, X. Xia, Z.-F. Jiang, B. Cheng, Y. Ning, F. Wang, Y. Zhao, X. Chen and J.-L. Zhang, *Angew. Chem., Int. Ed.*, 2022, **61**, e202208707.
28 S. V. Eliseeva, T. N. Nguyen, J. W. Kampf, E. R. Trivedi, V. L. Pecoraro and S. Petoud, *Chem. Sci.*, 2022, **13**, 2919–2931.
29 I. Martinić, S. V. Eliseeva, T. N. Nguyen, V. L. Pecoraro and S. Petoud, *J. Am. Chem. Soc.*, 2017, **139**, 8388–8391.
30 T. N. Nguyen, S. V. Eliseeva, I. Martinić, P. L. Carver, T. Lathion, S. Petoud and V. L. Pecoraro, *Chem. – Eur. J.*, 2023, **29**, e202300226.
31 C. M. Andolina, P. J. Klemm, W. C. I. I. I. Floyd, J. M. J. Fréchet and K. N. Raymond, *Macromolecules*, 2012, **45**, 8982–8990.
32 S. Plunkett, M. El Khatib, İ. Şencan, J. E. Porter, A. T. N. Kumar, J. E. Collins, S. Sakadžić and S. A. Vinogradov, *Nanoscale*, 2020, **12**, 2657–2672.
33 D. Kovacs, X. Lu, L. S. Mészáros, M. Ott, J. Andres and K. E. Borbas, *J. Am. Chem. Soc.*, 2017, **139**, 5756–5767.
34 A.-M. Caminade, A. Hameau, C.-O. Turrin, R. Laurent and J.-P. Majoral, *Coord. Chem. Rev.*, 2021, **430**, 213739.
35 M. D. Allendorf, C. A. Bauer, R. K. Bhakta and R. J. T. Houk, *Chem. Soc. Rev.*, 2009, **38**, 1330–1352.
36 A. Foucault-Collet, K. A. Gogick, K. A. White, S. Villette, A. Pallier, G. Collet, C. Kieda, T. Li, S. J. Geib, N. L. Rosi and S. Petoud, *Proc. Natl. Acad. Sci. U. S. A.*, 2013, **110**, 17199–17204.
37 J. Rocha, L. D. Carlos, F. A. A. Paz and D. Ananias, *Chem. Soc. Rev.*, 2011, **40**, 926–940.
38 H. Furukawa, K. E. Cordova, M. O'Keeffe and O. M. Yaghi, *Science*, 2013, **341**, 1230444.
39 H. Xu, M. Fang, C.-S. Cao, W.-Z. Qiao and B. Zhao, *Inorg. Chem.*, 2016, **55**, 4790–4794.
40 J. A. Smith, M. A. Singh-Wilmot, K. P. Carter, C. L. Cahill and J. A. Ridenour, *Cryst. Growth Des.*, 2019, **19**, 305–319.
41 G. Ji, J. Liu, X. Gao, W. Sun, J. Wang, S. Zhao and Z. Liu, *J. Mater. Chem. A*, 2017, **5**, 10200–10205.
42 T. W. Chamberlain, R. V. Perrella, T. M. Oliveira, P. C. de Sousa Filho and R. I. Walton, *Chem. – Eur. J.*, 2022, **28**, e202200410.
43 G. E. Gomez, R. Marin, A. N. Carneiro Neto, A. M. P. Botas, J. Ovens, A. A. Kitos, M. C. Bernini, L. D. Carlos, G. J. A. A. Soler-Illia and M. Murugesu, *Chem. Mater.*, 2020, **32**, 7458–7468.
44 A. Kourtellaris, W. Lafargue-Dit-Hauret, F. Massuyeau, C. Latouche, A. J. Tasiopoulos and H. Serier-Brault, *Adv. Opt. Mater.*, 2022, **10**, 2200484.
45 D. Andriotou, S. A. Diamantis, A. Zacharia, G. Itskos, N. Panagiotou, A. J. Tasiopoulos and T. Lazarides, *Molecules*, 2020, **25**, 523.

46 T. Feng, Y. Ye, X. Liu, H. Cui, Z. Li, Y. Zhang, B. Liang, H. Li and B. Chen, *Angew. Chem., Int. Ed.*, 2020, **59**, 21752–21757.
47 O. Guillou, C. Daiguebonne, G. Calvez and K. Bernot, *Acc. Chem. Res.*, 2016, **49**, 844–856.
48 K. Pei, J. Wu, M. Zhao, X. Feng, Y. Li, Y. Ma, H. Li and T. Zhai, *Adv. Opt. Mater.*, 2022, **10**, 2102143.
49 X. Yu, A. A. Ryadun, D. I. Pavlov, T. Y. Guselnikova, A. S. Potapov and V. P. Fedin, *Angew. Chem., Int. Ed.*, 2023, **62**, e202306680.
50 M. Pan, Y.-X. Zhu, K. Wu, L. Chen, Y.-J. Hou, S.-Y. Yin, H.-P. Wang, Y.-N. Fan and C.-Y. Su, *Angew. Chem., Int. Ed.*, 2017, **56**, 14582–14586.
51 D. Zhang, W. Zhou, Q. Liu and Z. Xia, *ACS Appl. Mater. Interfaces*, 2018, **10**, 27875–27884.
52 L. L. da Luz, R. Milani, J. F. Felix, I. R. B. Ribeiro, M. Talhavini, B. A. D. Neto, J. Chojnacki, M. O. Rodrigues and S. A. Júnior, *ACS Appl. Mater. Interfaces*, 2015, **7**, 27115–27123.
53 Z. Gao, B. Xu, T. Zhang, Z. Liu, W. Zhang, X. Sun, Y. Liu, X. Wang, Z. Wang, Y. Yan, F. Hu, X. Meng and Y. S. Zhao, *Angew. Chem., Int. Ed.*, 2020, **59**, 19060–19064.
54 Y. Wang, H. Li, X. He and Z. Xu, *Inorg. Chem.*, 2021, **60**, 15001–15009.
55 R. Cui, W. Sun, M. Liu, J. Shi and Z. Liu, *ACS Appl. Mater. Interfaces*, 2021, **13**, 59164–59173.
56 D. F. Sava Gallis, L. E. S. Rohwer, M. A. Rodriguez, M. C. Barnhart-Dailey, K. S. Butler, T. S. Luk, J. A. Timlin and K. W. Chapman, *ACS Appl. Mater. Interfaces*, 2017, **9**, 22268–22277.
57 X. Liu, R. Li, X. Xu, Y. Jiang, W. Zhu, Y. Yao, F. Li, X. Tao, S. Liu, W. Huang and Q. Zhao, *Adv. Mater.*, 2023, **35**, 2206741.
58 W. J. Rieter, K. M. L. Taylor and W. Lin, *J. Am. Chem. Soc.*, 2007, **129**, 9852–9853.
59 W. J. Rieter, K. M. L. Taylor, H. An, W. Lin and W. Lin, *J. Am. Chem. Soc.*, 2006, **128**, 9024–9025.
60 A. E. Psalti, D. Andriotou, S. A. Diamantis, A. Chatz-Giachia, A. Pournara, M. J. Manos, A. Hatzidimitriou and T. Lazarides, *Inorg. Chem.*, 2022, **61**, 11959–11972.
61 M. Seitz, A. G. Oliver and K. N. Raymond, *J. Am. Chem. Soc.*, 2007, **129**, 11153–11160.
62 S. A. Diamantis, A. Hatzidimitriou, A. K. Plessas, A. Pournara, M. J. Manos, G. S. Papaefstathiou and T. Lazarides, *Dalton Trans.*, 2020, **49**, 16736–16744.
63 T. N. Nguyen, G. Capano, A. Gładysiak, F. M. Ebrahim, S. V. Eliseeva, A. Chidambaram, B. Valizadeh, S. Petoud, B. Smit and K. C. Stylianou, *Chem. Commun.*, 2018, **54**, 6816–6819.
64 T. N. Nguyen, S. V. Eliseeva, A. Gładysiak, S. Petoud and K. C. Stylianou, *J. Mater. Chem. A*, 2020, **8**, 10188–10192.
65 V. Balzani, P. Ceroni and A. Juris, *Photochemistry and Photophysics: Concepts, Research, Applications*, Wiley, 2014.
66 M. Latva, H. Takalo, V.-M. Mukkala, C. Matachescu, J. C. Rodríguez-Ubis and J. Kankare, *J. Lumin.*, 1997, **75**, 149–169.
67 S. W. Thomas, G. D. Joly and T. M. Swager, *Chem. Rev.*, 2007, **107**, 1339–1386.
68 H.-J. Son, S. Jin, S. Patwardhan, S. J. Wezenberg, N. C. Jeong, M. So, C. E. Wilmer, A. A. Sarjeant, G. C. Schatz, R. Q. Snurr, O. K. Farha, G. P. Wiederrecht and J. T. Hupp, *J. Am. Chem. Soc.*, 2013, **135**, 862–869.
69 C. A. Kent, D. Liu, L. Ma, J. M. Papanikolas, T. J. Meyer and W. Lin, *J. Am. Chem. Soc.*, 2011, **133**, 12940–12943.